# Electronic Supplementary Information

# An Efficient Sensor for $Zn^{2+}$ and $Cu^{2+}$ Based on Different Binding Modes

**Jie Jiang, Huie Jiang, Xiaoliang Tang, Lizi Yang, Wei Dou, Weisheng Liu*, Ran Fang, Wei Liu**

*Key Laboratory of Nonferrous Metals Chemistry and Resources Utilization of Gansu Province and State Key Laboratory of Applied Organic Chemistry, College of Chemistry and Chemical Engineering, Lanzhou University, Lanzhou 730000, P. R. China*

**Corresponding author. Tel: +86-931-8915151*

*Fax number: +86-931-8912582*

*E-mail: liuws@lzu.edu.cn*

**Contents**

**Materials and Methods:** All reagents and solvents were obtained commercially and used without further purification unless otherwise noted. $^{1}$H NMR and $^{13}$C NMR spectra were recorded on a Bruker DRX400 spectrometer and referenced to solvent signals. Mass spectra (ESI) were performed on a LQC system (Finngan MAT, USA) using $CHCl_3$ as mobile phase. All UV—visible spectra and fluorescence spectra were recorded using a Varian Cary 100 spectrophotometer and Hitachi F—4500 luminescence spectrometer, respectively. The path length was 1 cm with cell volume of 3.0 mL. An excitation and emission slit of 5.0 nm were used for the measurements of fluorescence. All the detections of metal perchlorate salts were operated at pH = 7.14 maintained with tris—HCl buffer (10 mM Tris—HCl, 0.1 M $KNO_3$, 50% $CH_3CN$). The stock solution of **QA** was prepared in $CHCl_3$ (10 mM). Fluorescent quantum yields were determined to be 0.071 for **QA**, 0.132 for **QA**-$Zn^{2+}$ and 0.038 for **QA**-$Cu^{2+}$ by an absolute method using an integrating sphere on FLS920 of Edinburgh Instrument.

**CAUTION:** *Perchlorate salts with organic ligands can be potential explosive and should be handled with care.*

## 1.1 Synthesis of QA

**QA** was prepared according to the literature.[1] Yield: 77 mg (75 %). m.p. 237.1–237.6 °C. ESI-MS: m/z = 455.3 [M+H$^+$].

$^{1}$H NMR ($CDCl_3$, 400 MHz，ppm): $\delta$ 11.48 (s, 1H), 8.89 (dd, $J$ = 4.0 Hz, $J$ = 1.6Hz, 2H), 8.78 (dd, $J$ = 6.8 Hz, $J$ = 2.0 Hz, 2H), 8.17 (d, $J$ = 8.4 Hz, 2H), 7.54 (dd, $J$ = 15.6 Hz, $J$ = 8.4 Hz, 4H), 7.47 (dd, $J$ = 8.4 Hz, $J$ = 4.4 Hz, 2H), 3.39 (s, 4H), 2.92 (s, 8H).

$^{1}$C NMR ($CDCl_3$, 100 MHz， ppm): $\delta$ 168.96, 148.55, 139.00, 136.13, 134.29, 128.02, 127.24, 121.72, 121.57, 116.51, 62.49, 53.68.

## 1.2 Synthesis of QA-$Zn^{2+}$ and QA-$Cu^{2+}$

Complex of **QA**-$Zn^{2+}$: The reaction of **QA** (0.1 mmol) with Zn(II) perchlorates (0.2 mmol) in 5ml $CH_3CN/CHCl_3$ (1:1, V/V) for a few minutes afforded White solid. After the mixture was continually stirred for 2 h at room temperature, the precipitate was collected by filtration, washed with $CH_3CN/CHCl_3$ (1 : 1) three times, and dried in a vacuum. IR /$cm^{-1}$: 3457(OH), 1568(C=N), 1100(C-O). [2]

Complex of **QA**-$Cu^{2+}$: The reaction of **QA** (0.1 mmol) with Cu(II) perchlorates (0.2 mmol) in 5ml $CH_3CN/CHCl_3$ (1:1, V/V) for a few minutes afforded blue solid. After the mixture was continually stirred for 2 h at room temperature, the precipitate was collected by filtration, washed with $CH_3CN/CHCl_3$ (1 : 1) three times, and dried in a vacuum. IR /$cm^{-1}$: 1635(C=O), 1095(C-N).

# 2 UV—visible absorbance and fluorescence spectra

## 2.1

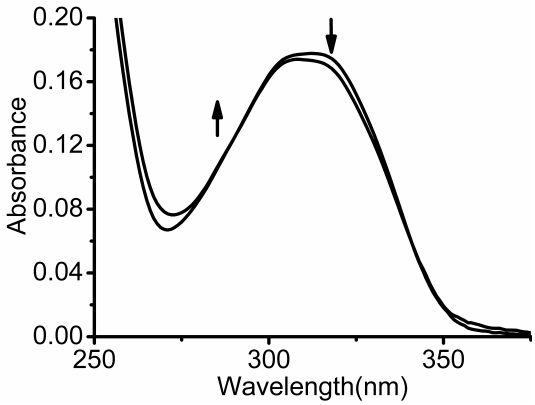


**Fig. S1** UV—Vis absorption spectra of **QA** (10 $\mu$M) in the presence of 40 $\mu$M $Zn^{2+}$ in buffer solution (10 mM Tris—HCl, 0.1 M $KNO_3$, 50% $CH_3CN$, pH = 7.14).

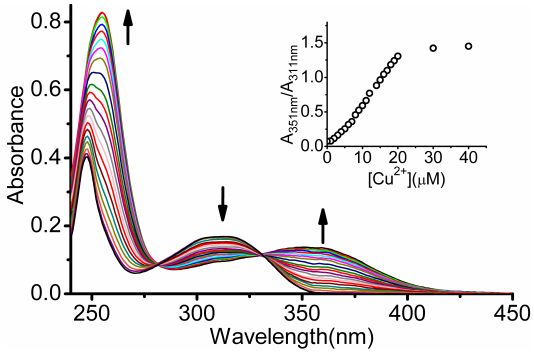


**Fig. S2** UV—Vis absorption spectra of **QA** in buffer solution (10 mM Tris—HCl, 0.1 M $KNO_3$, 50% $CH_3CN$, pH = 7.14) upon the titration of $Cu^{2+}$. $Cu^{2+}$ = 0—40 $\mu$M, [**QA**] = 10 $\mu$M. Inset: Ratiometric calibration curve $A_{351\ nm}$ / $A_{311\ nm}$ as a function of $Cu^{2+}$.

## 2.2


**Fig. S3** Fluorescence spectra of **QA** (1) in the presence of different metal ions $Li^{+}$ (2), $Na^{+}$ (3), $K^{+}$ (4), $Ca^{2+}$ (5), $Mg^{2+}$ (6), $Fe^{3+}$ (7), $Al^{3+}$ (8), $Cr^{3+}$ (9), $Co^{2+}$ (10) , $Ni^{2+}$ (11), $Cd^{2+}$ (12), $Ag^{+}$ (13), $Hg^{2+}$ (14), $Pb^{2+}$ (15), $Mn^{2+}$ (16), $Cu^{2+}$ (17) and $Zn^{2+}$ (18) (as their $ClO_4^-$ salts) in buffer solution (10 mM Tris–HCl, 0.1 M $KNO_3$, 50% $CH_3CN$, pH = 7.14). $\lambda_{ex}$ = 329 nm, [**QA**] = 10 $\mu$M, [$M^{n+}$] = 50 $\mu$M. Inset: Emission changes of **QA** (10 $\mu$M) in the presence of various amounts of $Zn^{2+}$ in buffer solution. (From **A** to **E**: [$Zn^{2+}$] = 20 $\mu$M, 10 $\mu$M, 2 $\mu$M, 1 $\mu$M and **QA** only.)


**Fig. S4** Absorption spectra of **QA** (1) in the presence of different metal ions $Li^{+}$ (2), $Na^{+}$ (3), $K^{+}$ (4), $Ca^{2+}$ (5), $Mg^{2+}$ (6), $Fe^{3+}$ (7), $Al^{3+}$ (8), $Cr^{3+}$ (9), $Co^{2+}$ (10) , $Ni^{2+}$ (11), $Cd^{2+}$ (12), $Ag^{+}$ (13), $Hg^{2+}$ (14), $Pb^{2+}$ (15), $Mn^{2+}$ (16), $Cu^{2+}$ (17) and $Zn^{2+}$ (18) (as their $ClO_4^-$ salts) in buffer solution (10 mM Tris–HCl, 0.1 M $KNO_3$, 50% $CH_3CN$, pH = 7.14). $\lambda_{ex}$ = 329 nm, [**QA**] = 10 $\mu$M, [$M^{n+}$] = 50 $\mu$M. Inset: Color changes of various amounts **QA**-$Cu^{2+}$ in buffer solution. (From **A** to **F**: [**QA**-$Cu^{2+}$] = 0 $\mu$M, 5 $\mu$M, 10 $\mu$M, 50 $\mu$M, 100 $\mu$M and 100 $\mu$M $Cu^{2+}$ only.)

## 2.3 Anions response experiments

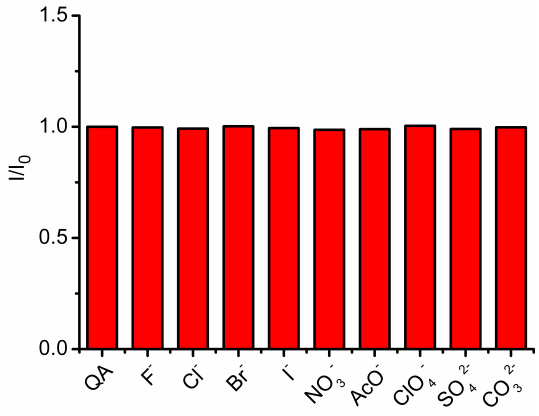


**Fig. S5** Fluorescence responses of probe **QA** (10 $\mu$M) in the presence of 10 equiv various anions: $F^-$, $Cl^-$, $Br^-$, $I^-$, $NO_3^-$, $ClO_4^-$, $AcO^-$, $SO_4^{2-}$ and $CO_3^{2-}$ (as their $Na^+$ salts) in buffer solution (10 mM Tris－HCl, 0.1 M $KNO_3$, 50% $CH_3CN$, pH = 7.14). Bars represent the ratio of the fluorescence intensity in the presence (I) and absence ($I_0$) of various anions at 402 nm. $\lambda_{ex}$ = 329 nm.

## 2.4 Other zinc and copper metal sources

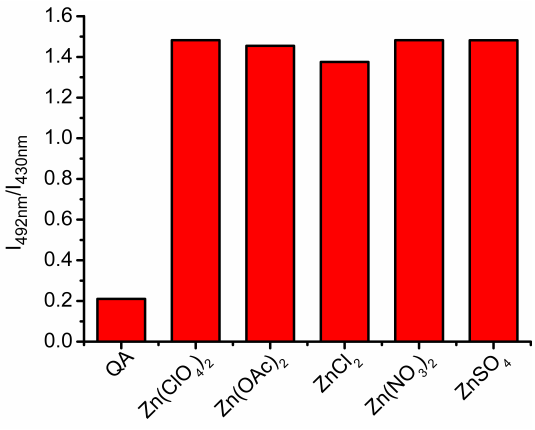


**Fig. S6** Fluorescence responses of 10 $\mu$M **QA** to zinc metal sources (20 $\mu$M): $Zn(ClO_4)_2$, $Zn(NO_3)_2$, $Zn(OAc)_2$, $ZnCl_2$, $ZnSO_4$ in buffer solution (10 mM Tris—HCl, 0.1 M $KNO_3$, 50% $CH_3CN$, pH = 7.14). Bars represent the ratio of thefluorescence intensity at 492 nm ($I_{492nm}$) over 430 nm ($I_{430nm}$). $\lambda_{ex}$ = 329 nm.

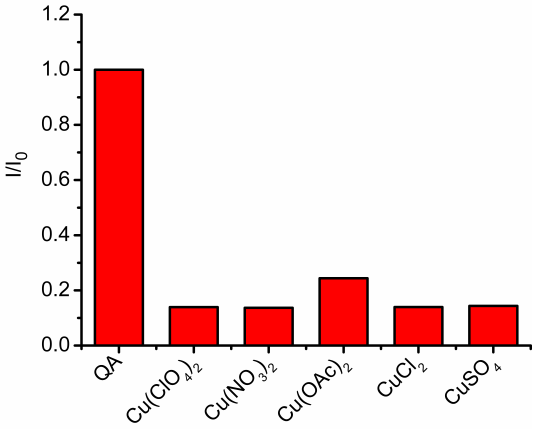


**Fig. S7** Fluorescence responses of 10 $\mu$M **QA** to copper metal sources (20 $\mu$M): $Cu(ClO_4)_2$, $Cu(NO_3)_2$, $Cu(OAc)_2$, $CuCl_2$, $CuSO_4$ in buffer solution (10 mM Tris—HCl, 0.1 M $KNO_3$, 50% $CH_3CN$, pH = 7.14). Bars represent the ratiofinal fluorescence intensity (I) over the original emission at 402 nm ($I_0$). $\lambda_{ex}$ = 329 nm.

## 2.5 Fluorescent titration experiment

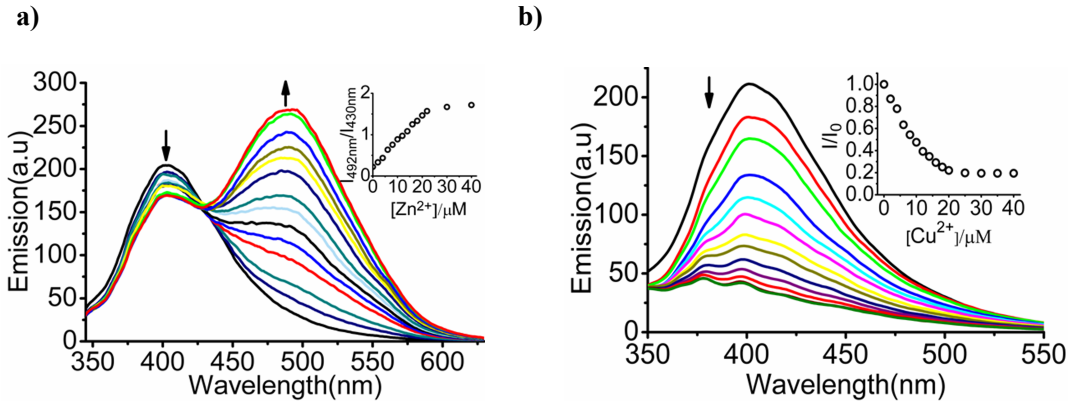


**Fig. S8** Fluorescence spectra of **QA** upon the titration of $Zn^{2+}$ (0–4 equiv) **a)** and $Cu^{2+}$ (0–4 equiv) **b)** in buffer solution (10 mM Tris–HCl, 0.1 M $KNO^3$, 50% $CH_3CN$, pH = 7.14). $\lambda_{ex}$ = 329 nm, [**QA**] = 10 $\mu$M. Inset: ratiometric calibration curve $I_{492\ nm}/I_{430\ nm}$ as a function of $Zn^{2+}$ **a)** and fluorescence intensity decrease ($I/I_0$) at 402 nm as a function of $Cu^{2+}$ **b)**.

## 2.6 Job's Plot

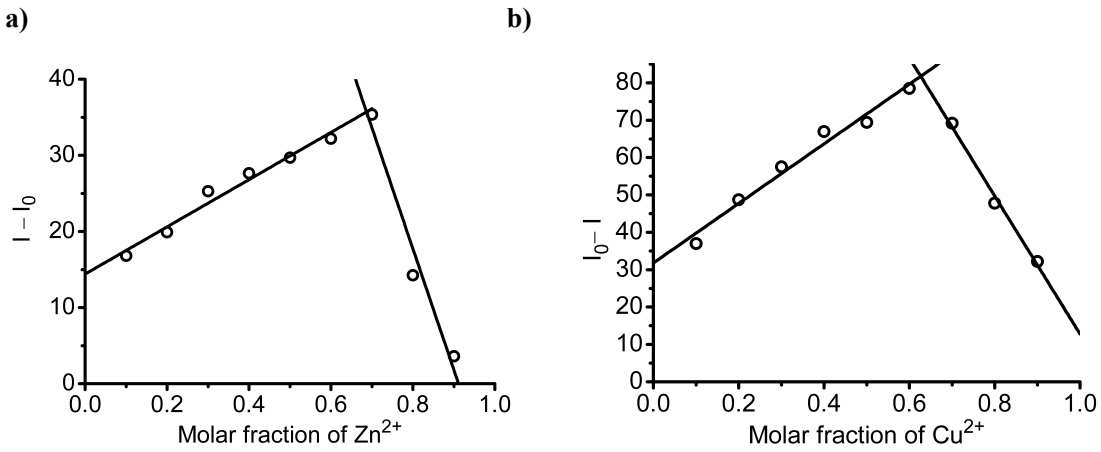


**Fig. S9 a)** Job's plot for **QA**-$Zn^{2+}$ (form 1 : 2 complex) in buffer solution. **b)** Job's plot for **QA**-$Cu^{2+}$ (form 1 : 2 complex) in buffer solution. The total [**QA**] + [$M(ClO_4)_2$] = 20 $\mu$M.

## 2.7 Ion competitive experiments

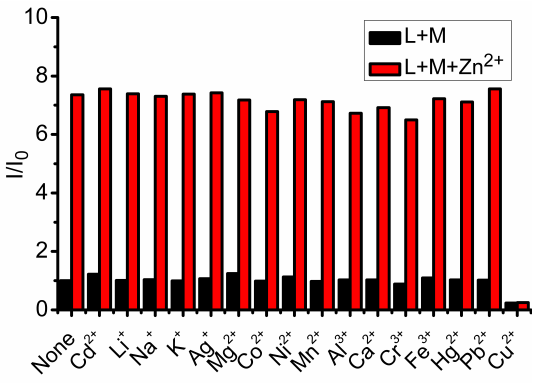


**Fig. S10** Fluorescence responses of 10 $\mu$M **QA** at 492nm to various metal cations in buffer solution (10 mM Tris—HCl, 0.1 M $KNO_3$, 50% $CH_3CN$, pH = 7.14). Bars represent thefinal fluorescence intensity at 492 nm (I) over the original emission at 492 nm ($I_0$). Black bars represent the addition of 5 equiv of metal ions to a 10 $\mu$M solution of **QA**. Red bars represent the subsequent addition of 5 equiv of $Zn^{2+}$ to the solution.

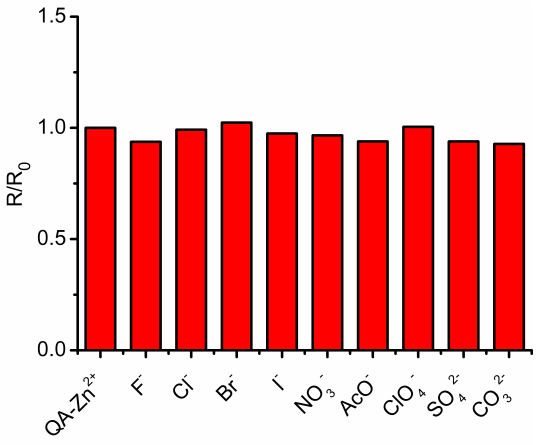


**Fig.S11** Fluorescence responses of probe **QA**-$Zn^{2+}$ system (10 $\mu$M) in the presence of 10 equiv various anions: $F^-$, $Cl^-$, $Br^-$, $I^-$, $NO_3^-$, $ClO_4^-$, $AcO^-$, $SO_4^{2-}$ and $CO_3^{2-}$ (as their $Na^+$ salts) in buffer solution (10 mM Tris—HCl, 0.1 M $KNO_3$, 50% $CH_3CN$, pH = 7.14). Bars represent the ratio of the fluorescence intensity ratio in the presence (R) and absence ($R_0$) of various anions. R = $I_{492nm}/I_{430nm}$, $\lambda_{ex}$ = 329 nm.

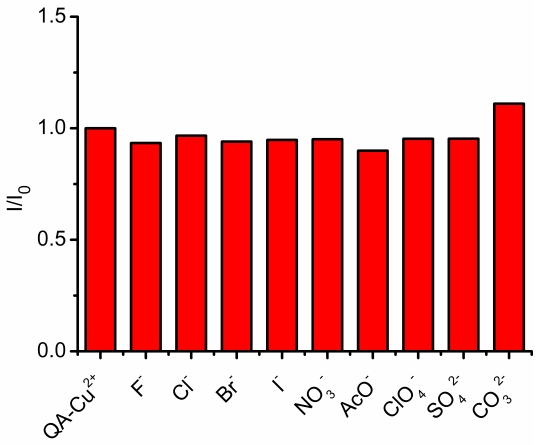


**Fig. S12** Fluorescence responses of probe **QA-**$Cu^{2+}$ system (10 $\mu$M) in the presence of 10 equiv various anions: $F^-$, $Cl^-$, $Br^-$, $I^-$, $NO_3^-$, $ClO_4^-$, $AcO^-$, $SO_4^{2-}$ and $CO_3^{2-}$ (as their $Na^+$ salts) in buffer solution (10 mM Tris—HCl, 0.1 M $KNO_3$, 50% $CH_3CN$, pH = 7.14). Bars represent the ratio of the fluorescence intensity in the presence (I) and absence ($I_0$) of various anions at 402 nm. $\lambda_{ex}$ = 329 nm.

## 2.8 pH effect

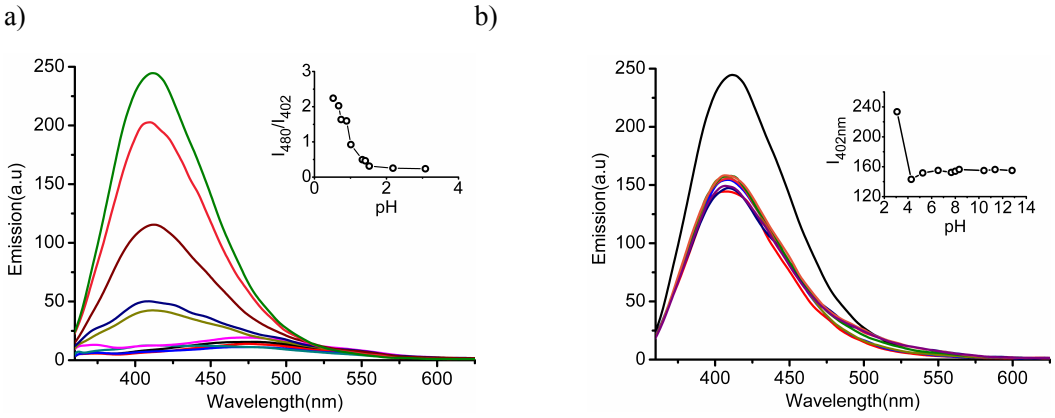


**Fig.S13** Influence of pH on the fluorescence of **QA** (10 $\mu$M) in 50% $CH_3CN$. **a)** pH 0.52–3.08. Inset: the ratiometric fluorescence changes as a function of pH; **b)** pH 3.08–12.8. Inset: the fluorescence intensity as a function of pH; $\lambda_{ex}$ = 329 nm.

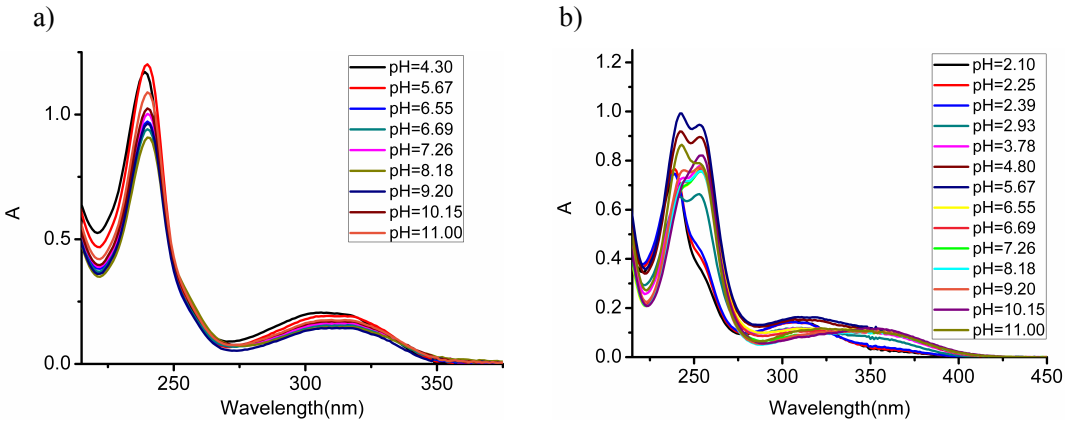


**Fig. S14 a)** Influence of pH on the absorption band of **QA**–$Zn^{2+}$(10 $\mu$M) in 50% $CH_3CN$. pH 4.30–11.00; **b)** Influence of pH on the absorption band of **QA**–$Cu^{2+}$(10 $\mu$M) in 50% $CH_3CN$. pH 2.10–11.00.

## 3. Determination of dissociation constant and stoichiometry of QA-$Zn^{2+}$ and QA-$Cu^{2+}$

The dissociation constant (defined as $K_d$) of **QA** complexing with $Zn^{2+}$ and $Cu^{2+}$ were studied by the following curve of fluorescence intensity ratio, which was obtained from the fluorescence titration spectra of **QA**. They were plotted according to the following equations:[3]

$$nM + L \Leftrightarrow M_nL \qquad \beta = \frac{[M_nL]}{[M]^n[L]} \qquad B = \log \beta$$

Where [M], [L] and [$M_n$L] are the concentrations of free $Zn^{2+}$ or $Cu^{2+}$, **QA** and **QA**-$Zn^{2+}$ or **QA**-$Cu^{2+}$; $\beta$ is total binding constant whose logarithmic form is defined as $B$.

The sigmoidal curve was obtained and the dissociation constant $K_d$ was deduced from ratiometric fluorimetric titration for $Zn^{2+}$ and direct fluorimetric titration for $Cu^{2+}$, respectively, according to the literature [4] (Fig.S15 and Fig.S16). And also, a Hill plot and a Hill coefficient can be gained (Fig.S17 and Fig.S18).

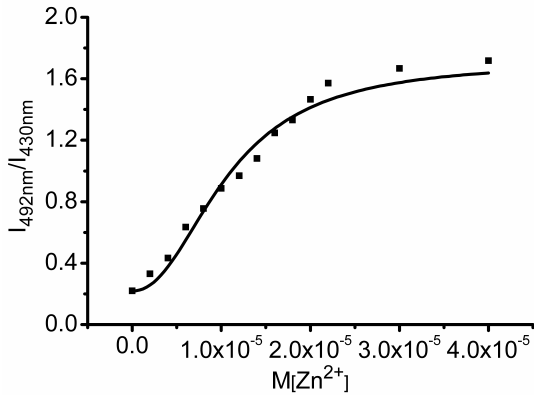


**Fig.S15** Curve of fluorescence intensity ratio (R= $I_{430\ nm}/I_{492\ nm}$) of **QA** versus increasing concentration of $Zn^{2+}$. $\lambda_{ex}$ = 329 nm, [**QA**] = 10 $\mu$M. The dissociation constant $K_d$ was deduced to be $(1.4 \pm 0.4) \times 10^{-11}$.

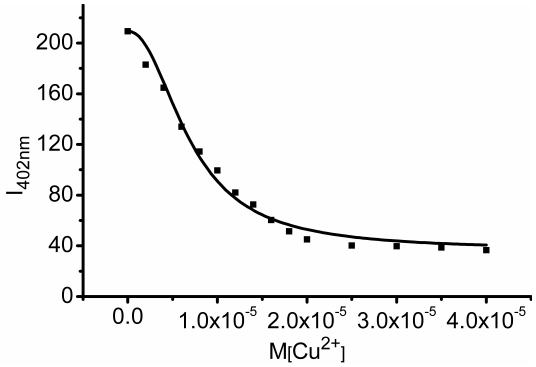


**Fig.S16** Curve of fluorescence intensity at 402 nm of **QA** versus increasing concentration of $Cu^{2+}$. $\lambda_{ex}$ = 329 nm, [**QA**] = 10 $\mu$M. The dissociation constant $K_d$ was deduced to be $(8.7 \pm 0.3) \times 10^{-12}$.

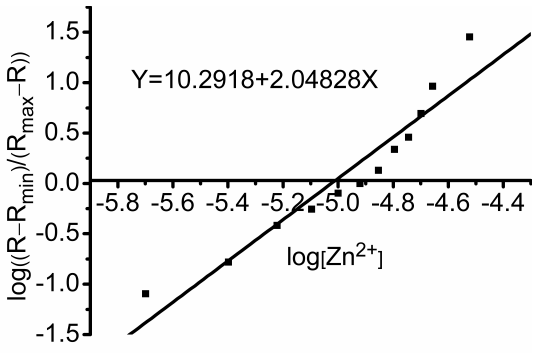


**Fig.S17** Fluorescence intensity intensity ratio (R= $I_{430\ nm}$ / $I_{492\ nm}$) of **QA** versus increasing concentration of log[$Zn^{2+}$]. $\lambda_{ex}$ = 329 nm, [**QA**] = 10 $\mu$M. The fluorescence response fits to a Hill coefficient of 2 (2.04828); It is consistent with the formation of a 1 : 2 stoichiometry for the **QA**-$Zn^{2+}$ complex.

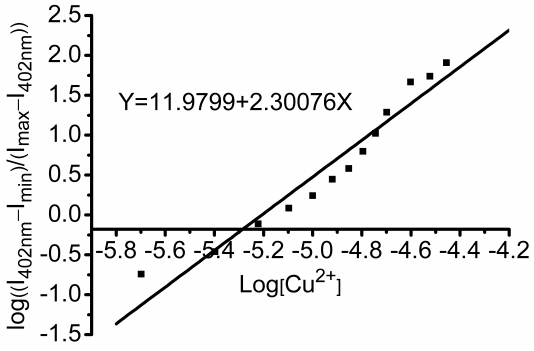


**Fig.S18** Fluorescence intensity at 402 nm of **QA** versus increasing concentration of log[$Cu^{2+}$]. $\lambda_{ex}$ = 329 nm, [**QA**] = 10 $\mu$M. The fluorescence response fits to a Hill coefficient of 2 (2.30076); It is consistent with the formation of a 1 : 2 stoichiometry for the **QA**-$Cu^{2+}$ complex.

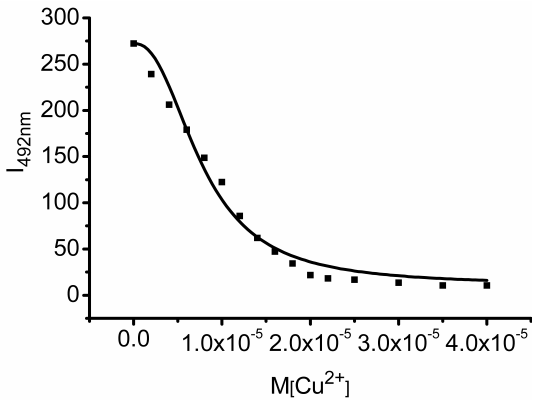


**Fig.S19** Curve of fluorescence intensity at 492 nm of **QA**-$Zn^{2+}$ versus increasing concentration of $Cu^{2+}$. $\lambda_{ex}$ = 329 nm, [**QA**-$Zn^{2+}$] = 10 $\mu$M. The dissociation constant $K_d$ was deduced to be (1.1 ± 0.7) × $10^{-12}$.

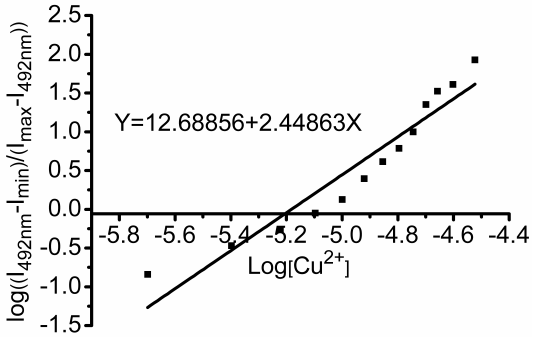


**Fig.S20** Fluorescence intensity at 492 nm of **QA**-$Zn^{2+}$ versus increasing concentration of log[$Cu^{2+}$]. $\lambda_{ex}$ = 329 nm, [**QA**-$Zn^{2+}$] = 10 $\mu$M. The fluorescence response fits to a Hill coefficient of 2 (2.44863); It is consistent with the formation of a 1 : 2 stoichiometry for the **QA**-$Cu^{2+}$ complex.

## 4. Determination of the detection limit

The detection limit was calculated based on the fluorescence titration. The fluorescence emission spectrum of **QA** was measured by ten times and the standard deviation of blank measurement was achieved. To gain the slop, the ratio of the fluorescence intensity at 492 nm to the fluorescence intensity at 430 nm ($I_{492nm}/I_{430nm}$) was plotted as a concentration of $Zn^{2+}$. So the detection limit was calculated with the following equation:

Detection limit = $3\sigma/k$

Where σ is the standard deviation of blank measurement, k is the slop between the fluorescence intensity ratios versus $Zn^{2+}$ concentration.

The detection limit of $Cu^{2+}$ both in the fluorescence titration experiment and displacement approach were measured similarly as above.

The detection limits for $Zn^{2+}$ and $Cu^{2+}$ in titration experiment were deduced to be 0.14 and 0.86 $\mu$M, respectively.

# 5. NMR Data

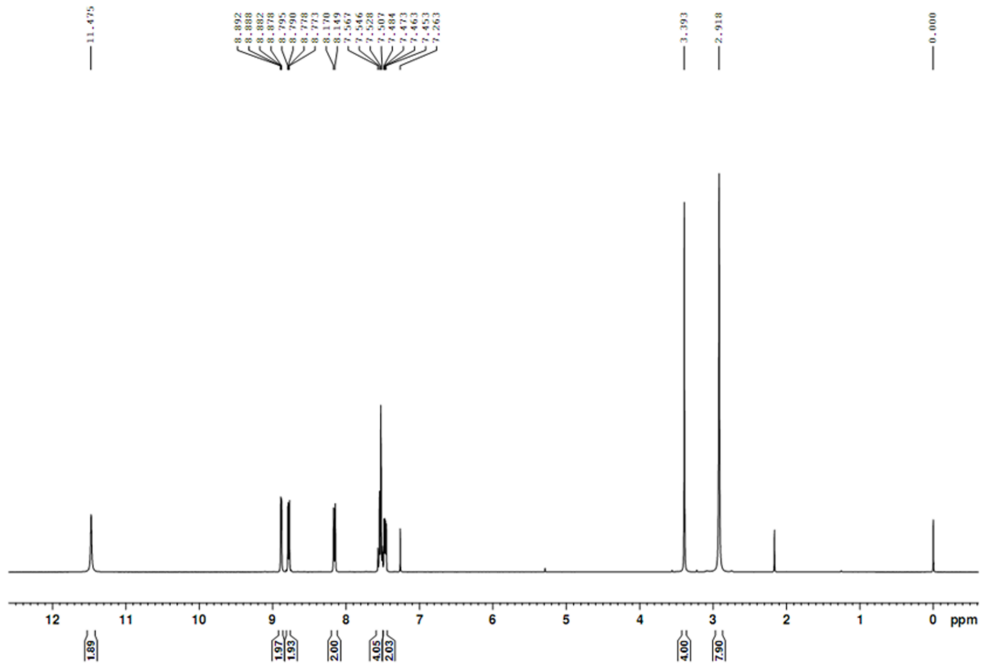


**Fig.S21** $^{1}$H NMR spectrum of **QA** ($CDCl_3$)

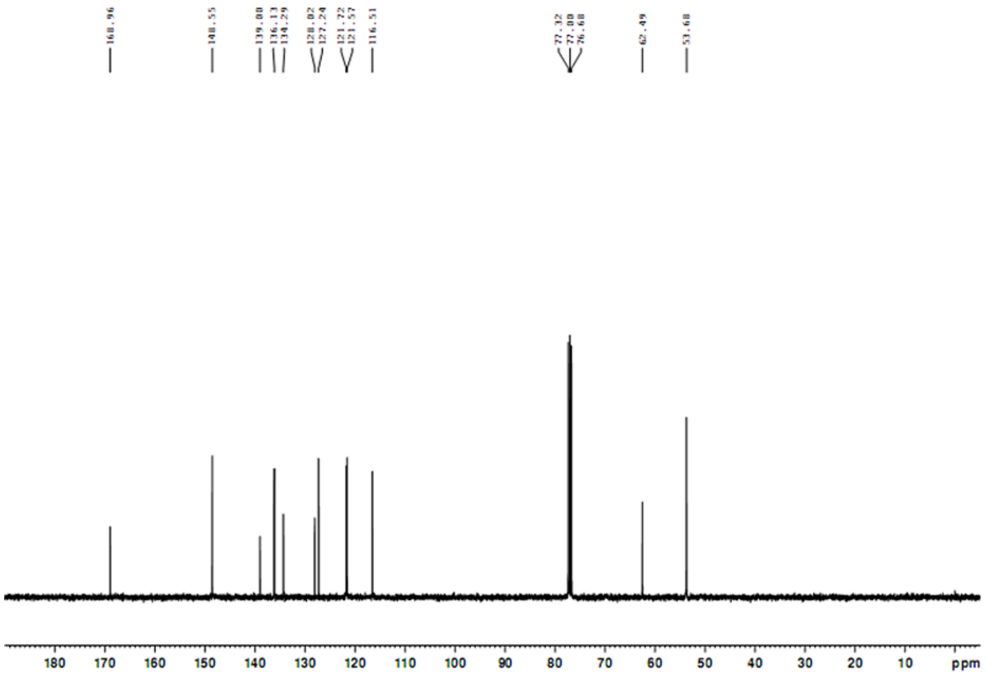


**Fig.S22** $^{13}$C NMR spectrum of **QA** ($CDCl_3$)

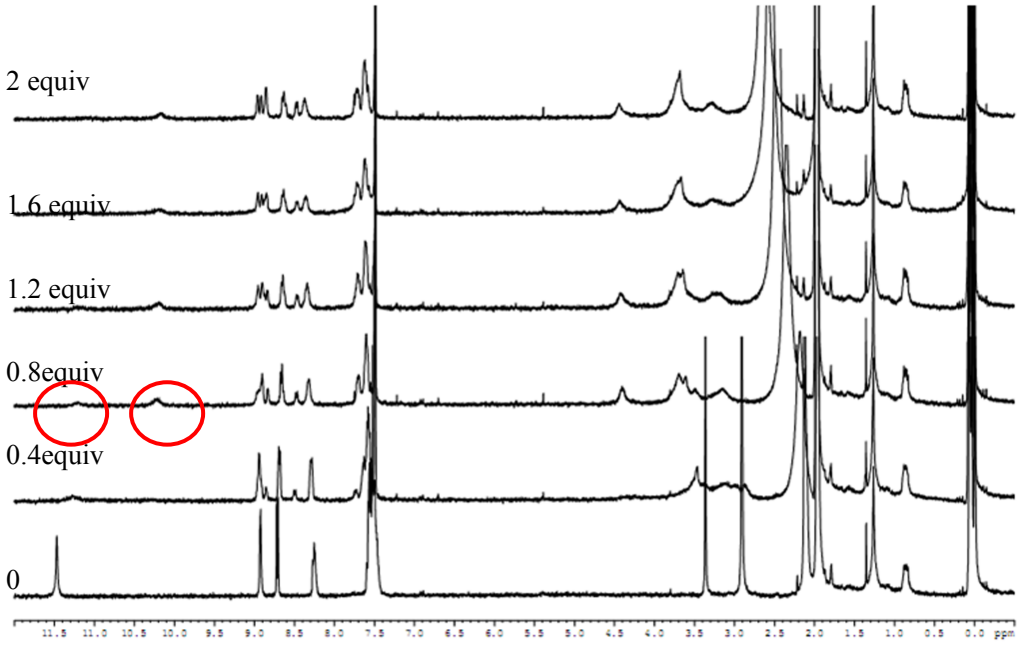


**Fig.S23** $^{1}$H NMR spectrum of **QA** in the presence of a different amount of $Zn^{2+}$ in $CD_3CN$ / $CDCl_3$ (2:3, v/v).

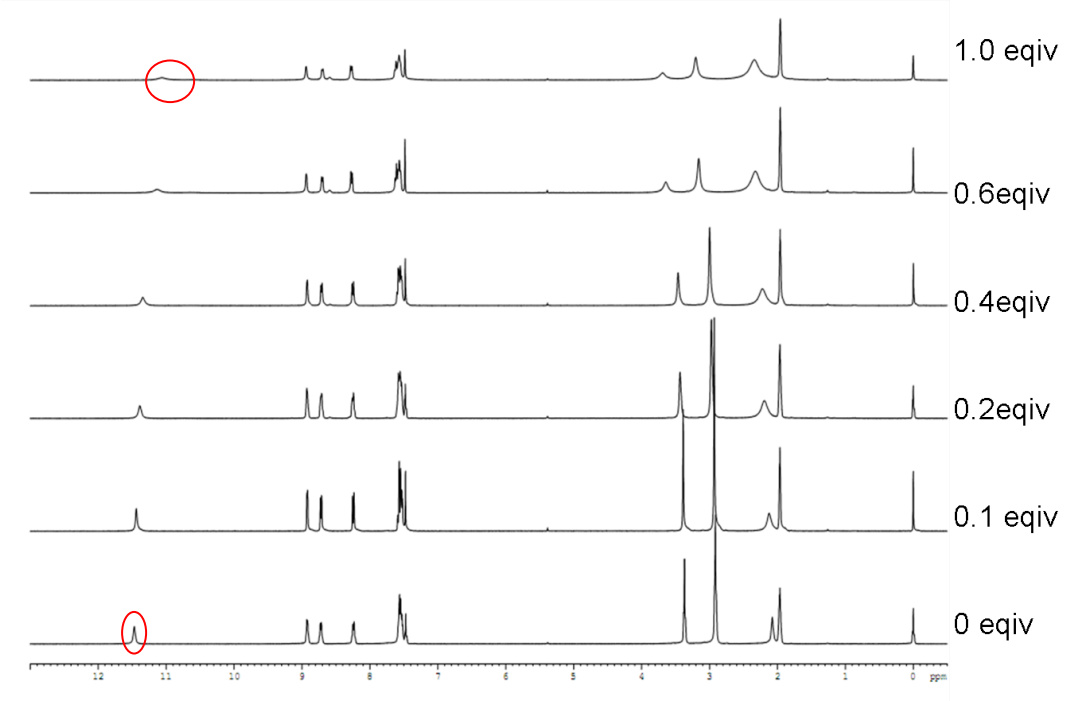


**Fig.S24** $^{1}$H NMR spectrum of **QA** in the presence of a different amount of $Cu^{2+}$ in $CD_3CN$ / $CDCl_3$ (2:3, v/v).

# 6. IR spectrum

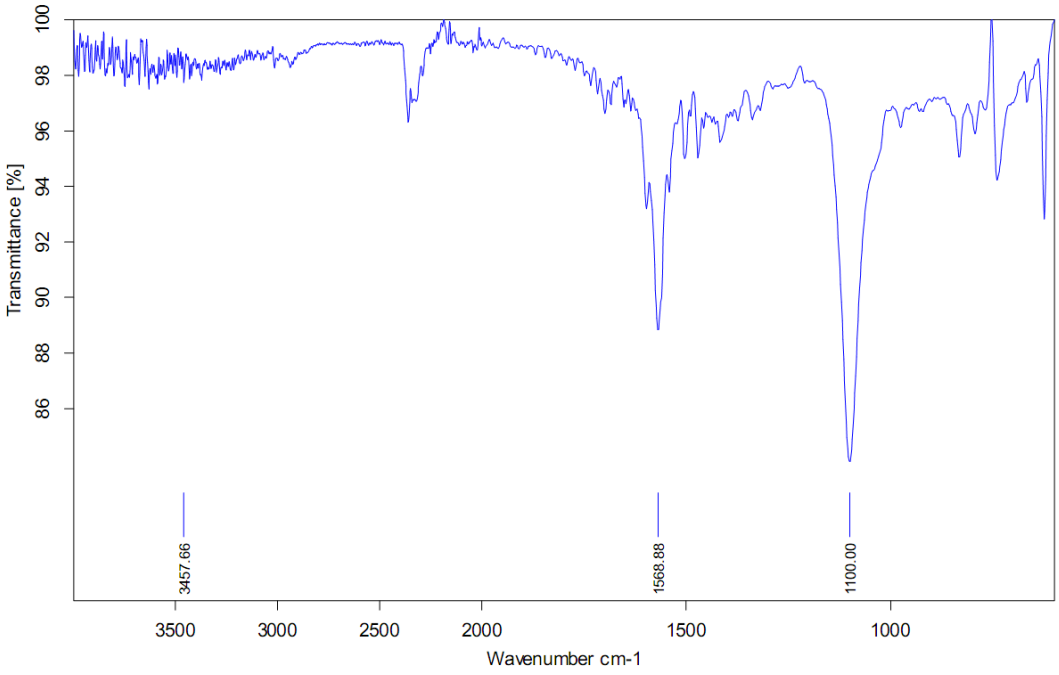


**Fig.S25** IR spectrum of **QA**–$Zn^{2+}$ (1:2) in $CH_3CN$ / $CHCl_3$ (1:1, v/v).

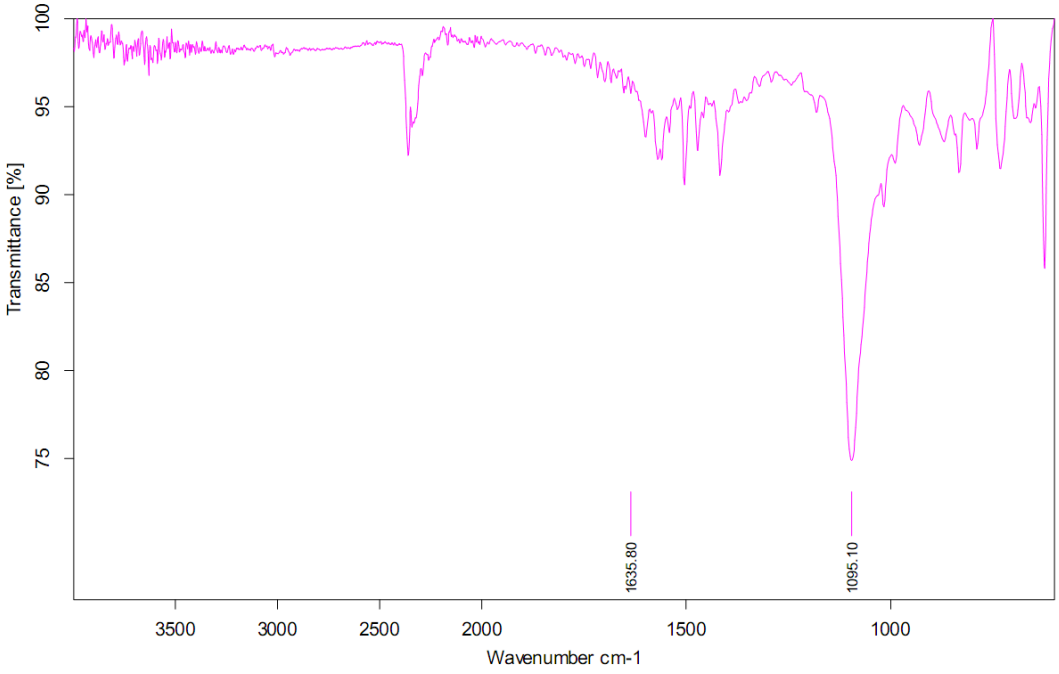


**Fig.S26** IR spectrum of **QA**–$Cu^{2+}$ (1:2) in $CH_3CN$ / $CHCl_3$ (1:1, v/v).

## 7. X-ray Crystallography

The single crystals for both **QA** and **QA**-$Cu^{2+}$ suitable for X-ray analysis were obtained by slow evaporation of the mixed solution after several days. The single crystals for **QA** were grown in chloroformand acetonitrile (1:1) mixture solvent, while those for **QA**-$Cu^{2+}$ were got in $CH_3CN$ / $CHCl_3$ / DMF (100 / 100 / 5 volume ratio) as component solvent.

The single-crystal X-ray diffraction measurements for both the two complexes were determined on a SMART APEX II CCD diffractometer equipped with a graphite crystal monochromatized Mo *Kα* radiation (λ = 0.71073Å) at 298(2) K. The structures were solved by direct methods and completed by iterative cycles of least-squares refinement. The H-atoms were placed in their geometrically calculated positions and treated as riding on the atoms to which they were attached. Absorption correction was employed using Semi-empirical methods from equivalents.[5] All details of the crystal parameters, data collection and refinements were listed in Table S1, representative bond lengths (Å) and angles (°) were presented in Table S2. Crystallographic data (without structure factors) for the structure reported in this paper has been deposited with the Cambridge Crystallographic Data Centre as supplementary publication no. CCDC (784130, 783720). Copies of these data can be obtained free of charge from the Cambridge Crystallographic Data Centre via http://www.ccdc.cam.ac.uk/cgi-bin/catreq.cgi.

**Table S1.** Crystal data and structure refinement for QA and QA-$Cu^{2+}$

| | **QA** | **QA**-$Cu^{2+}$ |
|---|---|---|
| Empirical formula | $C_{26}H_{26}N_6O_2$ | $C_{32}H_{42}N_8O_6Cu_2(ClO_4)_2$ |
| Formula Weight | 454.53 | 960.74 |
| Crystal color | colorless | blue |
| Wavelength (Å) | 0.71073 | 0.71073 |
| Crystal System | Triclinic | Triclinic |
| Space group | *P*-1 | *P*-1 |
| *Unitcell dimensions* | *a*(Å)=8.1803(11) *b*(Å)=8.7060(11) *c*(Å)=9.7467(13) *α*(°)=67.882(1) *β*(°)=79.756(1) *γ*(°)=65.593(1) | *a*(Å)= 8.438(8) *b*(Å)= 10.847(11) *c*(Å)= 11.262(11) *α*(°)= 86.424(12) *β*(°)= 73.054(11) *γ*(°)= 87.787(12) |
| *θ range* (°) | $2.3° < \theta < 25.5°$ | $2.5° < \theta < 25.5°$ |
| *Limiting indices* | $-9 \le h \le 9$, $-10 \le k \le 10$, $-10 \le l \le 11$ | $-10 \le h \le 10$, $-13 \le k \le 13$, $-13 \le l \le 8$ |
| *V* ( Å $^3$ ) | 585.38(13) | 983.9(17) |
| *Z* | 1 | 1 |
| *D*( calc )( g/cm $^3$ ) | 1.289 | 1.622 |
| *F*( 000 ) | 240 | 494 |
| $R_1$ [a][ I >2σ (I) ] | 0.0365 | 0.0599 |
| $wR_2$ [a] | 0.0979 | 0.1864 |
| Weighing scheme | $1/[\sigma^2(F_0)^2+(0.0477P)^2+0.1055P$ | $1/[\sigma^2(F_0)^2+(0.1231P)^2+0.8651P]$ |

]

[a] $R_1 = \sum||Fo|-|Fc||/\sum|Fo|$, $wR_2 = [\sum w(Fo^2-Fc^2)^2/\sum w(Fo^2)^2]^{1/2}$.

**Table S2.** Selected bond lengths (Å) and angles (°) for metal environments of **QA**-$Cu^{2+}$

| | | | | | |
|---|---|---|---|---|---|
| Cu(1)–O(2) | 1.969(5) | Cu(1)–O(3) | 2,263(5) | Cu(1)–N(1) | 2.003(5) |
| Cu(1)–N(2) | 1.914(5) | Cu(1)–N(3) | 2.077(5) | | |
| O(2)–Cu(1)–O(3) | 94. 29(19) | O(2)–Cu(1)–N(1) | 95. 79(19) | O(2)–Cu(1)–N(2) | 165. 8019 |
| O(2)–Cu(1)–N(3) | 94. 51(18) | O(3)–Cu(1)–N(1) | 92. 33(18) | O(3)–Cu(1)–N(2) | 99.88(19) |
| O(3)–Cu(1)–N(3) | 99. 73(17) | N(1)–Cu(1)–N(3) | 163. 49(18) | N(1)–Cu(1)–N(2) | 82.72(19) |
| N(2)–Cu(1)–N(3) | 84. 13(18) | | | | |

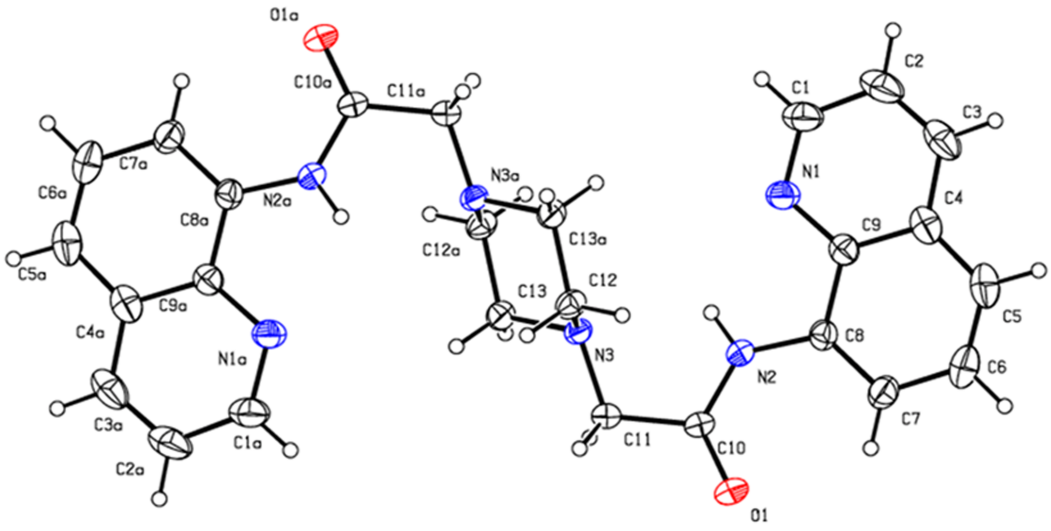


**Fig. S27** X-ray crystal structure of **QA** with thermal ellipsoids at the 30% probability level. Symmetry code: (a) 1-x, 1-y, -z.

**Reference**

(1) X. Guo, L. Jia, Y. Zhang, W. Si, S. Xu, Z. Xu, Faming Zhuanli Shenqing Gongkai Shuomingshu, 2009, CN 101440062.

(2) Z. Xu, K. H. Baek, H. Kim, J. Cui, X. Qian, D. Spring, I. Shin, J. Yoon, *J. Am. Chem. Soc.*, 2010, **132**, 601.

(3)B. Valeur, *Molecular Fluorescence: Principles and Applications,* Wiley-VCH, Weinheim, 2002.

(4) X. Tang, X. Peng, W. Dou, j. Mao, j. Zheng, W. Qin, W. Liu, J. Chang, X. Yao, *Org. Lett.* 2008, **10**, 3653; X. Peng, J. Du, J. Fan, J. Wang, Y. Wu, J. Zhao, S. Sun, T. Xu, *J. Am. Chem. Soc.* 2007, **129**, 1500; M. Baruah, W. Qin, R. A. L. Vallëe, D. Beljonne, T. Rohand, W. Dehaen, N. Boens, *Org. Lett.* 2005, **7**, 4377.

(5) R. Blessing, *Acta Crystallogr., Sect. A: Found. Crystallogr.* 1995, **A51**, 33.